Robust smart periodic truss

Leandro Rodrigues Cunha, Morvan Ouisse, Domingos Rade

Robust smart periodic truss

L.R. Cunha[1, 2], M. Ouisse[2], D.A. Rade[3]
[1] UFU, Federal University of Uberlandia, School of Mechanical Engineering
Av. João Naves de Ávila 2121, 38408-100, Uberlândia - MG, Brazil

[2] UBFC, University of Bourgogne Franche-Comté, Femto-st Institute, Department of Applied Mechanics
24 rue de l'épitaphe, Besançon, France

[3] ITA, Aeronautics Institute of Technology, Division of Mechanical Engineering
Praça Mal. Eduardo Gomes 50, 12229-900, São José dos Campos - SP, Brazil
Tel.: +55 (12) 39 47 58 63
E-mail: **rade@ita.br**

Abstract
Smart and periodic structures have received the attention of researchers by virtue of their great potential. These structures have powerful properties like adaptiveness and the ability to operate as mechanical filters. Although, the presence of uncertainties must be taken into account to guarantee robustness. Thus, a finite element model is proposed to elucidate the importance of stochastic aspects and to present the concept of robust frequency bandgap. The smart part consists of piezoelectric actuators connected to resonant circuits in a tridimensional truss unit cell. The periodic part is the replication of this cell to assemble the final structure. Floquet/Bloch conditions are used to model the infinite representation. Then, a Monte Carlo Simulation is carried out and the bandgaps' bounds are analyzed considering frequency responses and dispersion diagrams. The goal being to evaluate the influence of uncertainties affecting the prediction of the attenuation zones. Likewise, the consequences of increasing the uncertainty level are evaluated.

1 Introduction

Wave propagation [1] is one of the basis of vibration analysis. If this type of propagating energy arrives in a boundary condition or regardless of the impedance mismatch nature, there is a part that will be reflected and another transmitted. The presence of this kind of discontinuity, located periodically in a structure, can creates destructive interferences and, consequently, this movement is blocked and this energy is trapped inside this periodicity. Repetitive or periodic structures have being recently in focus by researchers of vibration control scientific community. It is explained by this unusual mechanical filter behavior for wave dispersion. A detailed review about these kinds of structures can be found in [3] and some overviews about their future in [4]. One of these perspectives is related to adaptiveness and tunable frequency bandgaps.

Smart material and structures capacity of self-sensing and self-changing to adapt to new conditions according to design requirements is their most important characteristic. Some fundamental aspects of these intriguing structures can be found in [21]. Therefore, periodic and smart structures seem to be a good combination to help the resolution of complex vibration problems. More information about periodic and smart structures is shown in [5] and [6].

Piezoelectric (PZT) actuators [21, 22, 30] are used in the numerical example of this study. If this actuator is linked in series with a shunt circuit, it will dynamically behaves as adding a Dynamic Vibration Absorber (DVA). This kind of mechanism creates resonant bandgaps if placed periodically in a structure. More information about DVAs can be found in [7, 8, 9]. The principle behind this strategy is that the vibrational energy is transformed into electric energy through the direct piezoelectric effect and is transferred to the circuit where it is partially dissipated and/or dispersed. Among the types of used electric circuit, RL, known

as resonant circuits, are considered as some of the most efficient [22, 23]. Such circuits comprise an inductor and a resistor that are connected to the piezoelectric transducer that is assimilated to a capacitor, thus forming an RLC circuit. When coupled to a dynamic system, this device operates similarly to a dynamic vibration absorber (DVA). Distributing these devices may lead to multimodal control [24].

Claeys describes the difference between placing a localized mass and a DVA in a periodic structure in [10]. Normally, increasing the mass density in one specific degree of freedom (dof) in a unit cell may create a large band gap but with weak attenuation. Oppositely, by adding a spring-mass dof, it is possible to create resonant band gaps whose attenuation zones are narrower but with strong dispersion grace of lower frequency response amplitudes. Although, as it is not yet possible to add just an inertia effect on an electrical circuit with a PZT actuator, because only the actuator is already a spring equivalent, the resonant circuit is the best choice. The main advantage of using piezoelectric actuators, rather than DVAs, is the characteristic of no addition of significant mass to the main structure and the convenience of electronically tuning without changing geometric properties. Moreover, these circuits can be redesigned and unusual behaviors can be included. One example of this is the negative capacitance shunting [13], which aims at removing the intrinsic capacitive effect of the piezoelectric patch [25]. This may be combined with resonant circuits [26], opening the way to new strategies with wideband efficiency [27, 28, 29].

Signorelli in [11] and [12] shows the wave propagation behavior in truss structures by using beam finite element and the transfer matrix method. This sort of structure also has the weightlessness as its major characteristic. In virtue of this, the use of piezoelectric actuator in these lattices like structures seems to be a good compromise because it favors the lightness design requirements. Nevertheless, uncertainty and robustness analysis are rare in literature. Near-periodic structures, defects, impurities on periodic structures and the localization phenomena are well detailed by [16, 17, 18, 19], but robustness analysis are scarce.

In this paper, one addresses the robustness of repetitive truss structures whose attenuation zones are created and passively controlled by using piezoelectric stack actuators associated with electrical shunt circuits [21, 22]. The finite element method is used to find the movement equation for unit cells [31, 32] whose three members contain a piezoelectric stack actuator connected to this circuit. Just like DVAs, shunt circuits must be tuned, which means that the values of their electric parameters must be precisely chosen for vibration attenuation in a narrow frequency band. However, the characteristic values of electronic components are prone to variability, due to manufacturing process and temperature, which can lead to mistuning and, consequently, decreasing of the control performance.

In this scenario, it becomes essential to evaluate the probability that the system will comply with the design requirements, given the probability density functions ascribed to the uncertain variables considered. For that, three different cases are analyzed based on typical operation and performance requirements. Uncertainties in the values of mass joints and inductance of the shunt circuit are modeled as Gaussian random variables. Following, a Monte Carlo Simulation [33, 34, 35] is performed considering an infinite and a finite model by using the dispersion constants and frequency response function bandgaps data as output variables. The uncertainty level is varied by increasing the standard deviation of input variables as a percentage of their means. Subsequently, the results are presented and discussed.

2 Methodology

A unit cell is the smallest part of a periodic structure that is repeated side by side to assemble the complete structure. As long as these cells are identical, appropriate periodic boundary conditions can be taken into account and an infinite model can be created. The equation (1) presents the Floquet [2] theorem for a 1D periodic structure:

$$X(x+l) = \lambda X(x), \tag{1}$$

where, in an equivalent mechanical structure, X can be the displacement, x the position, l the cell length, or spatial period, and λ is the Floquet multiplier. For example, using a discrete model, the periodic boundary conditions are described in equations (2) and (3):

$$u_R^{(i)} = u_L^{(i+1)} = e^{\mu} u_L^{(i)}, \tag{2}$$

$$f_R^{(i)} = -f_L^{(i+1)} = -e^{\mu} f_L^{(i)}, \tag{3}$$

for continuity and equilibrium to the left (L) and right (R) of the unit cell, respectively, where μ is the dispersion constant with δ and ε its real and imaginary components. These variables are the attenuation and phase constants, respectively [3, 4]. For a purely complex μ, the waves propagate and the frequency zone is a pass band. If, in a given frequency band, all waves correspond to purely real values of μ, the waves are attenuated and this zone is a stop band or well kwon in periodic structure scientific community as bandgap.

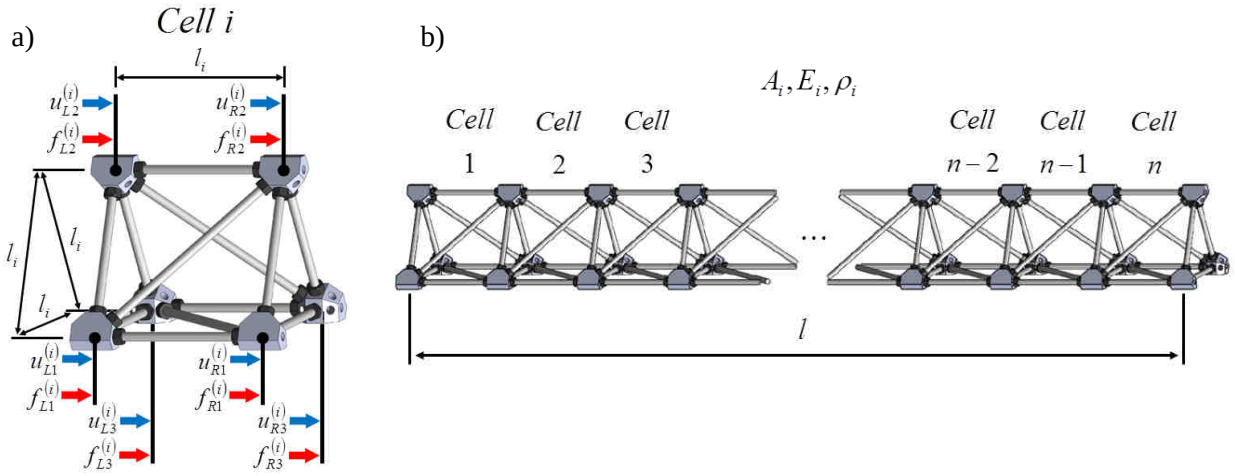

Figure 1: a) 3D truss unit cell and b) its finite model.

In this article, a simple truss unit cell, composed of 12 longitudinal rods, is shown in Figure 1. The embedded smart devices will be described in the next section. This structure has 3 boundary nodes on each side, the rods' properties are the (common) cross section area A, the Young's modulus E, density ρ and we denote l_i the length of the cell i while l is the total length of a structure with n cells. For a sake of simplicity and low computational cost, the repetitive truss structure in Figure 1 is composed only by bar finite elements with 2 nodes and 3 degrees of freedom (dof) per node.

2.1 Smart Cell

One category of smart material are the piezoelectric material [21]. These materials produce an electrical output when a mechanical strain is imposed. This effect is called direct. Oppositely, a mechanical strain can also be induced by applying an electrical signal to this material and it is reciprocally called the inverse effect. These properties are expressed mathematically by the following equation:

$$\begin{Bmatrix} D \\ S \end{Bmatrix} = \begin{bmatrix} \varepsilon_{33}^{T} & d_{33} \\ d_{33} & s^{E} \end{bmatrix} \begin{Bmatrix} E \\ T \end{Bmatrix}, \tag{4}$$

where D and S are the electric displacement and the mechanical strain, E and T are the electrical field and mechanical stress. The material properties $\varepsilon_{33}^{T}(F/m)$, d_{33} (C/N or V/m) and s^{E} (m²/N) are, respectively, the dielectric permittivity coefficient, piezoelectric strain coefficient and the mechanical compliance of the piezoelectric material of the active members. The indexes E and T represent the values in short-circuit (constant electric field) and open-circuit (varying electric field) with stress-free condition, while 33 is the direction along the axis of piezoelectric material polarization and it is one of the most common operating modes of a piezoelectric device. These characteristics are used to model the semi-active finite element present on this repetitive structure.

2.1.1 Periodic Cell with a resonant shunt circuit

In this section, the representation of the finite element model of the three-dimensional truss cell is depicted in Figure 2. This unit cell is composed by 6 nodes, 9 passive elements and 3 active elements. The nodes displacement are connected and the joint has a spherical function. Each of the active members is considered as being composed of a stack-type actuator placed between two passive segments. The actuator is assumed to be composed of piezoelectric discs poled in the axial direction (direction 3), wired in such a way that those discs are electrically connected in parallel. Application of voltages to the actuators will generate an internal longitudinal force enabling to attenuate transversal and longitudinal waves in the truss.

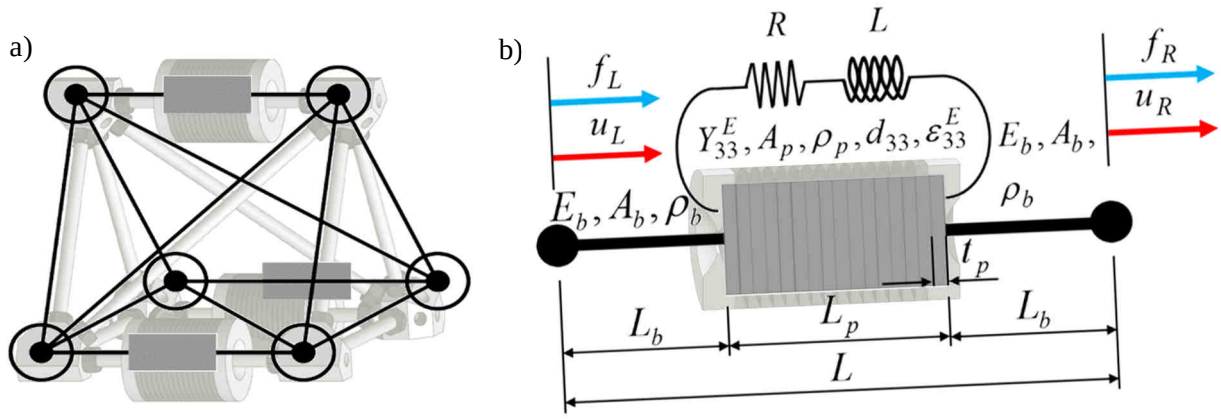

Figure 2: a) Smart unit cell and b) its piezoelectric stack actuator described as a finite element model.

As indicated in Figure 2, E (N/m^2), A (m^2) and ρ (kg/m) are the Young's modulus, cross-section area and linear mass density of the passive members, respectively. The others properties, Y_{33}^{E} (N/m^2), A_p (m^2), t_p (m) and ρ_p (kg/m) are the Young's modulus, cross-section area, thickness of the piezoelectric discs and linear mass density of the piezoelectric material of the active members. The physical and geometrical properties of the main structure and the actuator are provided in Table 1, in which subscripts b and p indicate the properties related to the metallic and piezoelectric material.

Property	Unit	Symbol	Steel (b)	PZT-5H (p)
Young's modulus	$[N/m^2]$	E_i and Y_{33}^{E}	2.1×10^{11}	60.0×10^{9}
Density	$[kg/m^2]$	ρ_i, ρ_b or ρ_p	7860.0	7800.0
Cross section area	$[m^2]$	A_i, A_b or A_p	25.0×10^{-6}	27.5×10^{-6}
Bar lengths (Cell length)	$[m]$	L_b or L_p (L or l_i)	0.033 (0.1)	0.033 (0.1)
Piezoelectric strain coefficient	$[C/N]$ or $[V/m]$	d_{33}	-	650.0×10^{-12}
Dielectric permittivity coefficient	$[F/m]$	ε_{33}^{T}	-	33.0×10^{-9}

Table 1: Properties of the smart periodic cells.

As detailed in reference [21, 22] the development of the finite element-based equations of motion of the electromechanical system can be made and it is equivalently expressed as:

$$\mathbf{M}\ddot{\mathbf{U}}(t)+\mathbf{K}\mathbf{U}(t)-\tilde{\mathbf{K}}V(t)=\mathbf{F}(t), \tag{5}$$

$$\tilde{\mathbf{K}}\mathbf{U}(t)+\mathbf{\Gamma}V(t)=Q(t), \tag{6}$$

where $\mathbf{M}$ is the mass matrix, $\mathbf{K}$ is the stiffness matrix, $\tilde{\mathbf{K}}$ is the electromechanical coupling matrix, $\mathbf{F}$ is the vector of external loads, $\mathbf{\Gamma}$ is the matrix of dielectric permittivity, $\mathbf{U}$ is the vector of mechanical degrees of freedom, $Q(t)$ is the electric charge and $V(t)$ is the voltage across the electrodes of the piezoelectric patches. The main structures is considered as conservative and the damping matrix $\mathbf{C}$ is zero. A RLC shunt circuit can be connect in series by adding the voltage condition as described in equation (7).

$$V(t)=R\dot{Q}(t)+L\ddot{Q}(t). \tag{7}$$

Associating Eqs. (5), (6) and (7), the electromechanical equations of motion are found under the form:

$$\overline{\mathbf{M}}\ddot{\mathbf{Z}}(t)+\overline{\mathbf{C}}\dot{\mathbf{Z}}(t)+\overline{\mathbf{K}}\mathbf{Z}(t)=\overline{\mathbf{F}}(t), \tag{8}$$

where $\mathbf{Z}(t)$, $\overline{\mathbf{M}}$, $\overline{\mathbf{C}}$ and $\overline{\mathbf{K}}$ are equal to $\{\mathbf{U}(t) \quad Q(t)\}^T$, $\left[\mathbf{M} \quad \mathbf{0}; -L\tilde{\mathbf{K}} \quad L\mathbf{\Gamma}\right]^T$, $\left[\mathbf{0} \quad \mathbf{0}; -R\tilde{\mathbf{K}} \quad R\mathbf{\Gamma}\right]^T$ and $\left[\mathbf{K} \quad \tilde{\mathbf{K}}^T; \mathbf{0} \quad -\mathbf{I}\right]^T$, respectively. An equivalent movement equation of a truss model can be found in [22]. In this work, Preumont shows a method by using the admittance of the shunt circuit.

2.1.2 Tuning a resonant RLC circuit

Figure 2 b) illustrates a piezoelectric transducer connected to a resonant (RL) shunt circuit and bonded to a host vibrating structure. Similarly to what happens with a dynamic vibration absorber, the resonant shunt circuits must be tuned, which means that the values of their electrical resistance and inductance parameters must be accurately determined for the attenuation of vibrations of the host structure in a given range of frequencies. According to Hagood and Von Flotow [22], the electromechanical coupling coefficient K_{ij} plays the same role as the mass ratio in tuning a DVA. Indeed, this coefficient can be approximated as follows: $K_{ij}^2=\left(\left(\omega_n^D\right)^2-\left(\omega_n^E\right)^2\right)/\left(\omega_n^E\right)^2$ where ω_n^D and ω_n^E are the n-th natural frequencies in open and closed circuit, respectively. Knowing the value of K_{ij}, one can calculate the optimum values of resistance R_{opt} and inductance L_{opt} according to: $r_{opt}=\left(\sqrt{2}K_{ij}\right)/\left(1+K_{ij}^2\right)$, $R_{opt}=r_{opt}/\left(C^S\omega_n^E\right)$, $\delta_{opt}=\sqrt{1+K_{ij}^2}$ and $L_{opt}=\left(\left(\omega_n^E\right)^2C^S\right)^{-1}$. In this article, the electrical resistance is considered as 0 and no optimal values are used to tune. Thus, equation (9) shows how the inductance value is obtained for a specific tune frequency:

$$L=\frac{1}{\omega_n^2C^S}. \tag{9}$$

However, in practical conditions, the values of the electric characteristics of the shunt circuit are inevitably affected by uncertainties resulting from material composition, manufacturing process and temperature variations. Such uncertainties can lead to mistuning of the shunt circuit and, as a result, deterioration of the performance of the damping/resonating device. In the case of periodic structures, it changes the bandgap

bounds and, for as strong impedance mismatch in mechanical and electrical domains can creates natural frequencies inside that increases the amplitude and, consequently, decrease the attenuation zone efficacy.

2.2 Frequency Response Function and Dispersion Diagrams

To give a sense on the influence of the joint mass and shunt inductance, 8 scenarios were compared by observing the dispersion diagrams and frequency responses and they are illustrated in Figure 3.

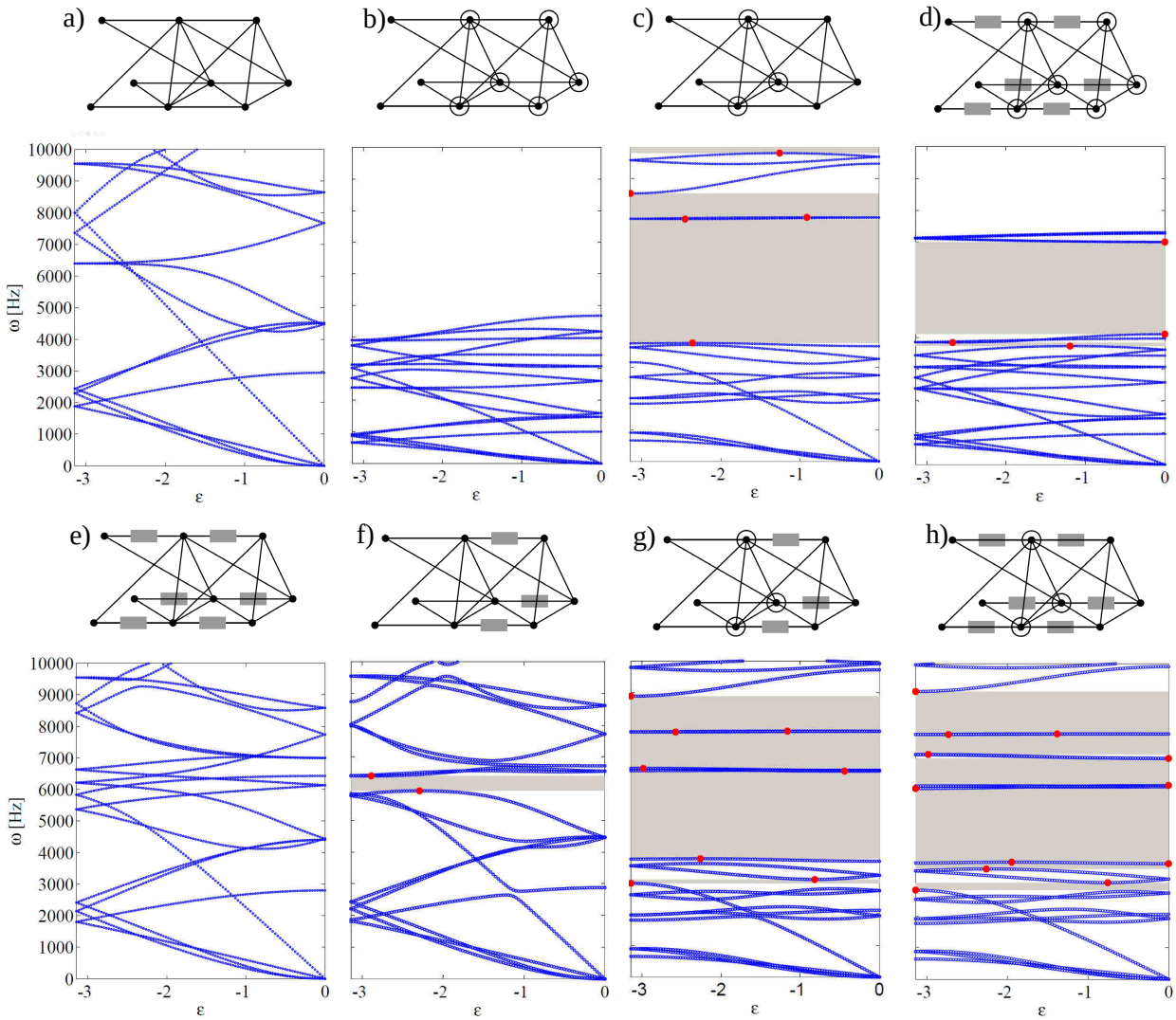

Figure 3: Considered unit cells a), b), c), d), e), f), g) and h) with their respective dispersion diagrams.

The equation 8 can be solved considering a harmonic solution to obtain the frequency response function (FRF) in equation (10). Moreover, the equation (11) is achieved by solving equation (10) considering periodic boundary conditions of equations (2) and (3).

$$\overline{\mathbf{H}}(\omega) = \left(-\omega^2\overline{\mathbf{M}} + j\omega\overline{\mathbf{C}} + \overline{\mathbf{K}}\right)^{-1}, \tag{10}$$

$$\left[\overline{\mathbf{K}}^{(r)}(\mu) + j\omega\overline{\mathbf{C}}^{(r)} - \omega^2\overline{\mathbf{M}}^{(r)}(\mu)\right]\ \mathbf{U}^{(r)}(\mu) = 0\,. \tag{11}$$

Figures 3 a), b), c), d), e), f), g) and h) shows the added mass and actuator position with their correspondent imaginary part of dispersion constants. Transversal and longitudinal wave's modes are not sorted and the bandgaps highlighted in gray comprehend these two kind of waves. The red dots indicate the bandgap

bounds. It is important to mention that as the model of one cell has 18 and 21 d.o.f., considering reduced matrices (r), the same number of mode branches can be found. As long as it does not represent all the dof that one finite structure can have, the area after the last branch is not considered as an attenuation zone and they are not exposed in these diagrams. The Figure 4 shows their equivalent respective frequency response by considering a transversal (x or y) and longitudinal (z) excitation on the first node cell and observing the response of equivalent node of last cell.

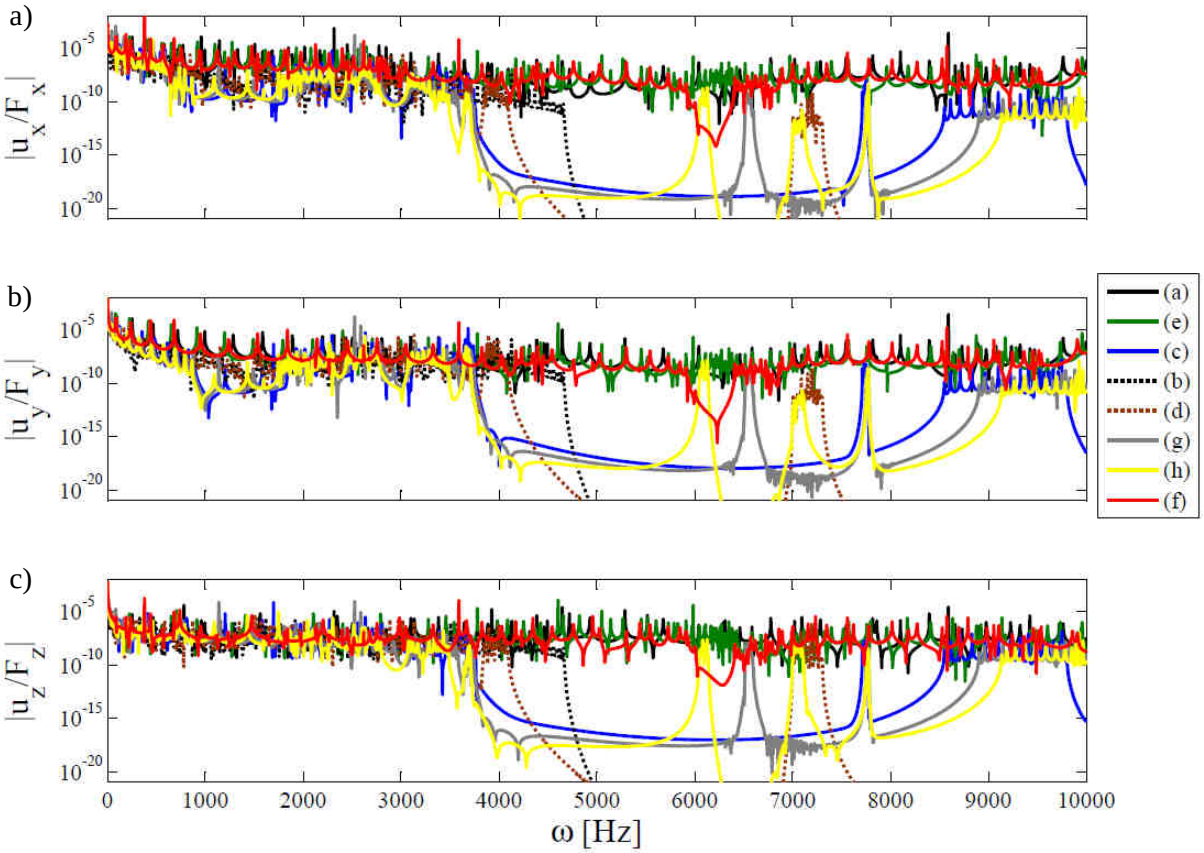

Figure 4: a), b) and c) frequency responses of these periodic finite structures with 10 cells by exciting the first node on direction x, y and z and observing the correspondent dofs on the last unit cell.

The number of cells considered to model the finite structure is equal to 10. This choice was done concerning the lowest number of cells that the bandgap is easily depicted in frequency response.

The added mass (m_a) is equal to 0.3 kg and the value of the inductance (L) to tune to a 7000 Hz, considering equation (9) is 0.1084 H.

It is possible to observe that infinite and finite models have the same band gaps and it is verified by comparing Figures 3 and 4. Some important aspects can be observed. Firstly, these models without added joint mass and piezoelectric actuator have no band gaps (Figure 3.a). The same can be observed by adding mass in all joint or adding actuators as shown in Figures 3 b) and 3 e). The fact of adding mass in joints, or considering the actuators in half cell, creates the attenuation zones that can be analyzed in Figures 3 c) and 3 f). By comparing these diagrams, a larger one is found in the case of added mass and a deeper one with added mass and PZT in shunt circuit. It is similar to the added mass and mass-spring effects in [10].

Figures 3 d), g) and h) are the combination of the others. The bandgap width is increased by combining added mass and actuator in scenarios of figures 3 g) and 3 h). Uncertainties can drastically change these bandgaps behavior and it is elucidate in the following.

2.3 Monte Carlo Simulation and Localization Phenomena

The Monte Carlo Simulation (MCS) [33, 34 and 35] is a method that consists in sampling input random variables, defined as a probability density function, to obtain predefined outputs. As mentioned in reference [33], convergence can be reached with approximately 95% confidence, by using from 10,000 to 20,000 samples, depending on the function being evaluated. This convergence is characterized by the stabilization of mean and standard deviation values. For problems featuring low standard deviations, very large numbers of samples are necessary. Optimized sampling methods can be used to reduce the computation effort necessary for MCS convergence. In this work, the sampling technique referred as Latin Hypercube Sampling (LHS) was used. More details about this technique can be found in reference [36].

A specific probability density function should be chosen to represent the stochastic variable considering the input variable characteristics. In this article, for the sake of simplicity and easy comprehension, the normal distribution is used. Considering a Gaussian distribution, if the standard deviation has high values, the gap between the properties of neighbor cells can creates the localization phenomena.

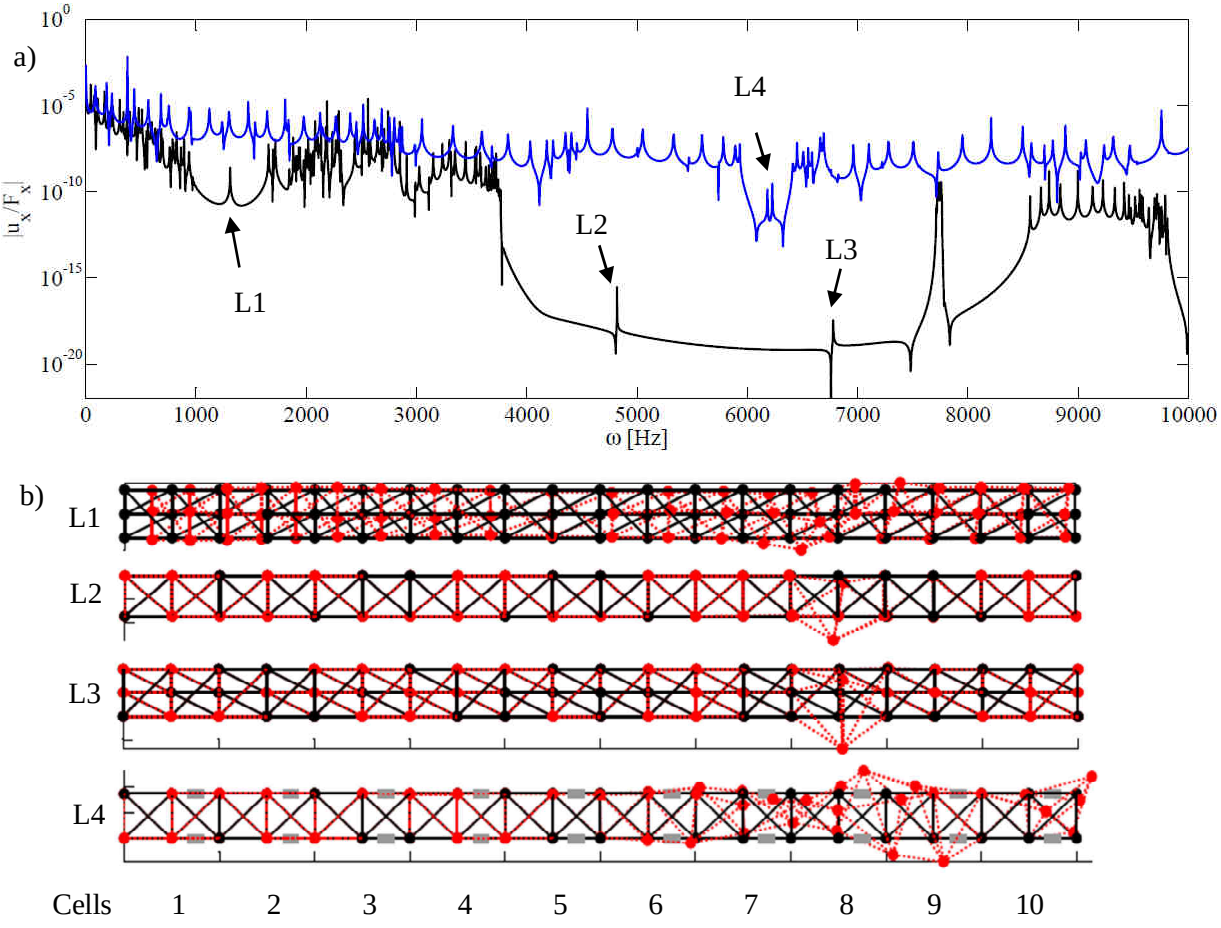

Figure 5: a) FRFs with localization phenomena L1, L2, L3 and L4 and b) their correspondent mode shape.

The Figure 5 a) shows two FRFs considering a strong difference between one or two cells and the others in the same structure. L1, L2 and L3 are the localization phenomena by adding a mass of 1 kg on dofs 142, 143 and 144 located in cell 8. L4 is the same but by changing the inductance of cells 8 and 9 to 0.001 H. The Figure 5 b) depicts their respective mode shapes and it can be observed that the displacement of nodes in these places is higher than the other positions of finite structure.

The localization phenomena can be briefly explained as normal mode that is confined in a specific place of the structure. As the number of cells tends to infinity, the influence of this mode tends to zero. Consequently, it does not appear in the infinite model. It is explained due to the stronger impedance mismatch compared

to other cells and, grace of it, the localization phenomenon appears. These phenomena can be considered as valuables as long as they reduce the variation of bandgap borders.

In other words, this kind of unpredictable event in a Monte Carlo Sampling adds robustness to the bandgap behavior in meanings of borders variation but it becomes hard to observe the amplitude on FRF inside bandgaps' zones and to identify the effective attenuation zones. Consequently, a robust interval confidence envelope will not take into account the localization phenomena since the worst configuration may takes part in any cell in a random analysis.

3 Numerical Example

In practice, it is not easy to design locally or to modulate periodically the inertia and the stiffness of a mechanical structure without weakening it. Normally, the properties as Young modulus and the density do not vary considerably if the material comes from same pack. Therefore, the principal incoming of uncertainties are the imperfections or defects caused by the manufacturing process. Accordingly, Figures 3 (c), (f) and (h) illustrate the 3 situations of interest in which the added joint mass and inductance values are stochastically analyzed. The Table 1 shows the properties of the truss unit cell for the numerical example.

3.1 Probabilistic Analysis

A periodic structure is composed by quasi-identical cells. This "quasi" is for the reason that there is no perfectly identical structures even they were designed to be. Thus, a robustness analysis is employed for this periodic structure with the goal of finding a robust bandgap. For this case, to get closer to reality, the variables of each cell should be independents. For the sake of comparison, infinite and finite models are used in this probabilistic analysis. To realize this investigation, for each standard deviation of random input variable (RV), a convergence of Monte Carlo Simulation is achieved and the outputs are obtained. In this article, the band gap edges are the outputs. Figures 3 show an illustration of these variables where the red dots are the bounds for infinite structure and a specified magnitude, different for each case, is used as a threshold for obtaining the bandgaps limits for a finite structure. The stochastic properties of the input random are shown in Table 2.

	Variables	Distribution	Mean (μ)	Standard Deviation (σ)
X_1	m_a $[kg]$	Normal (Gaussian)	0.3	$\gamma \times \mu_{X_1}$
X_2	L $[H]$	Normal (Gaussian)	0.1084	$\gamma \times \mu_{X_2}$

Table 2: Probabilistic variables and their distributions.

Two different cases are considered for each of the 3 scenarios of figures 3 c), f) and g):

- the uncertainty variable (1 RV) in the unit cell is repeated for each cell and, consequently, the structure still periodic (infinite model);
- all cells are independents (10 RV) from the uncertainty point of view (the structure is not perfectly periodic anymore, meaning quasiperiodicity, and is strictly finite).

For both cases, FE models were considered. The equation (12) presents the stochastic coefficient γ. It permits the variation of uncertainty level, given by the standard deviation, which is obtained from a percentage of probability distribution mean, according to:

$$\sigma_{X_n} = \gamma \times \mu_{X_n} \ . \tag{12}$$

This parameter varies from 2 % to 20 % with a step of 2 % for this numerical example. Then, for each considered value, a Monte Carlo Simulation with Latin Hypercube is performed until its convergence (number of samples around 5000). Considering a Normal approach for 95% of confidence level envelope, the output standard deviation value must multiplied by 1.96. It means that the probability of the output mean of the output samples has 95% of chance to be in this interval.

4 Numerical Results

The Figure 6 shows the envelope of the frequency band gaps for three considered scenarios. Figures 6 a), b) and c) for infinite model obtained from imaginary part of propagation constant considering with 1 RV (strictly periodic structure) and Figures d), e) and f) for finite model obtained from frequency responses with 10 RV (quasi-periodic structure).

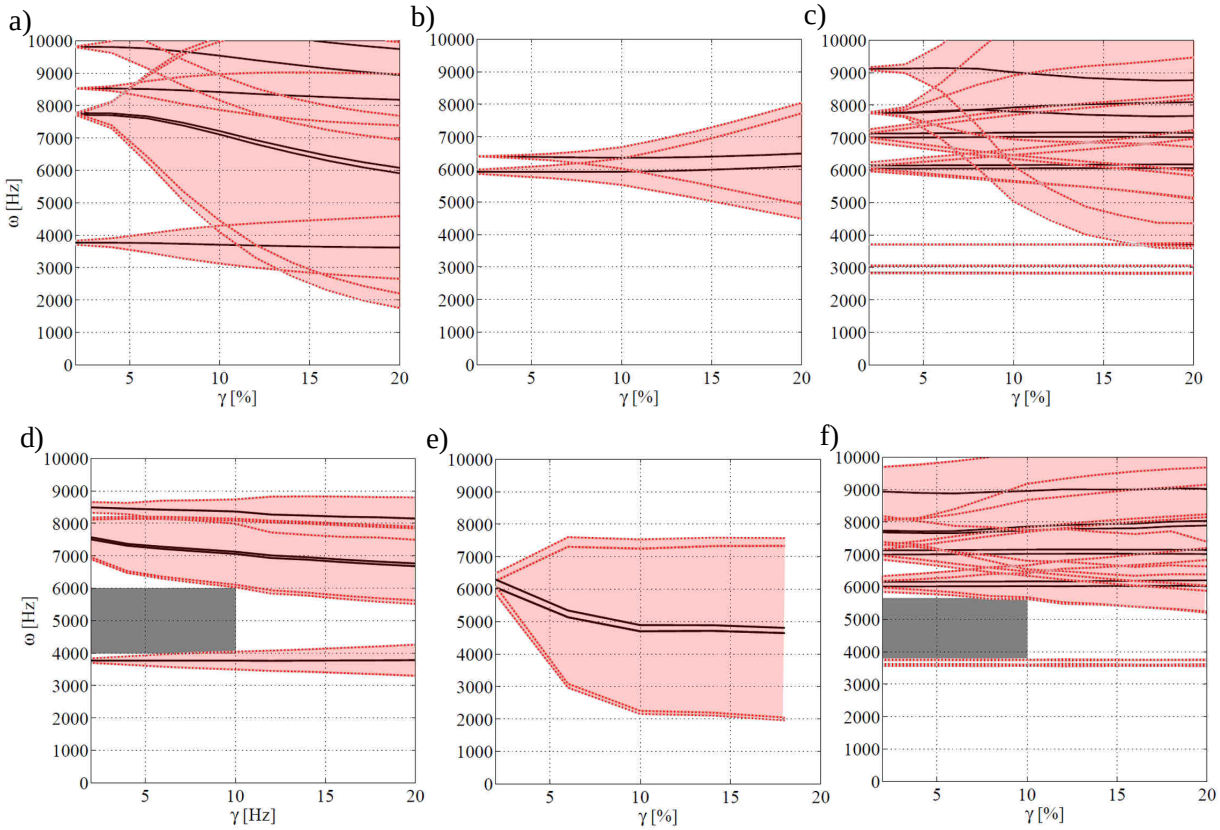

Figure 6: Bandgap bounds envelopes relatives to (c), (f) and (h) on figure 3, with: a) mass as RV, b) and c) inductance as RV considering an infinite model (1 RV) with their correspondent d), e) and f) to finite model results with 10 RV.

Considering a normal approach, this picture shows the means and the 95% confidence intervals. It is possible to observe that the envelopes widths increase according to the increasing of uncertainty level. In general, the envelopes are narrower for the models with finite structures (10 RV), approximately less than a half of the bandgaps obtained with infinite structures (1 RV).

If an uncertainty level of 10 % is considered for the random variables, the dark gray areas represents the robust bandgaps (bandgap almost certain considering these uncertainties).

The localization phenomena perturbed the result in Figure 6 e) and equivalent results were not found as related to Figures 6 d) and 6 f). This proves that this phenomenon is strongly sensible to low variations of inductance values in a shunt circuit and an erroneous result is obtained.

The Figure 7 elucidates the concept of robust band gap by situating the classical band gaps and robust band gaps inside the frequency response and dispersion diagrams, for infinite and finite models, respectively.

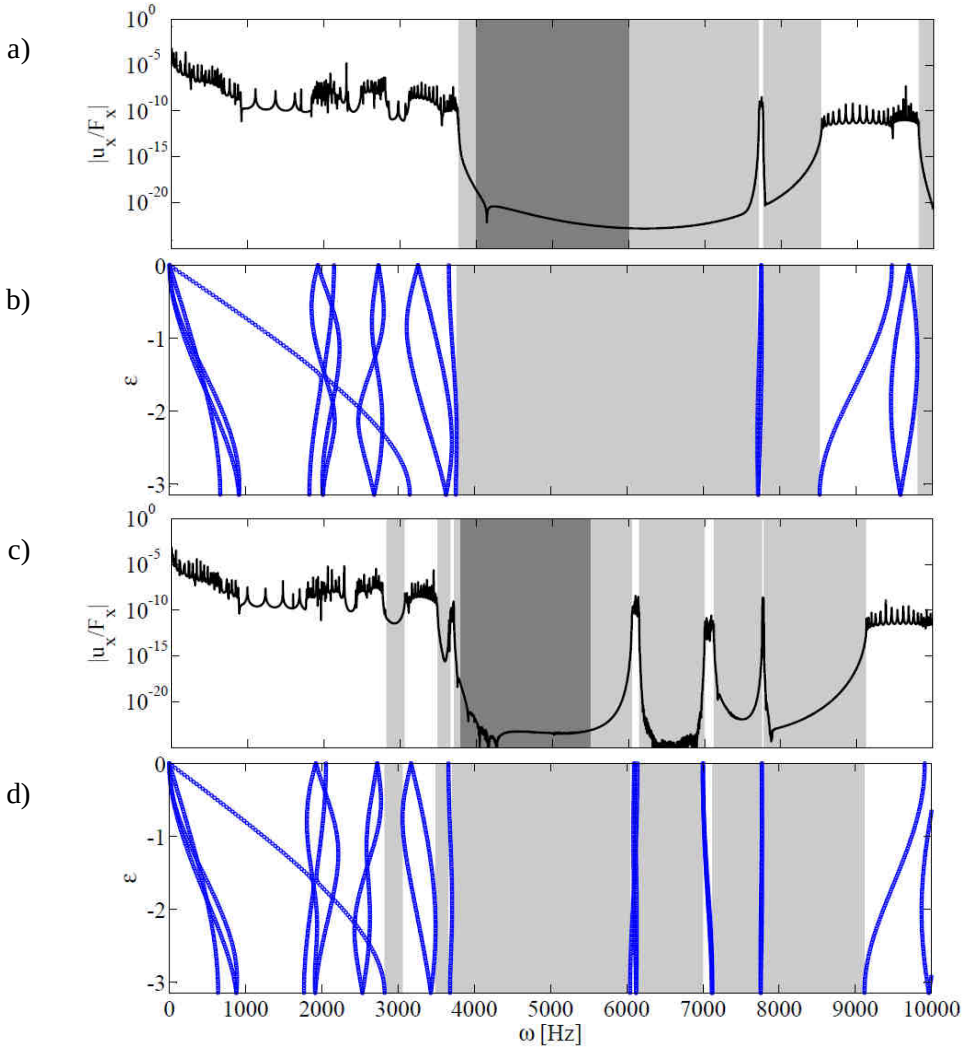

Figure 7: a), b), c) and d) Robust band gaps for a) finite and b) infinite structures.

The light red areas (envelopes) in Figure 6 indicate that the attenuation zone calculated with a single random variable is narrower than the dark gray, which was obtained with ten random variables for gamma, considering γ equals to 10%. Thus, when one uncertainty is considered for each cell of a finite structure, which corresponds to the quasi-real case, the effects on the responses are compensated and the structure are intrinsically more robust. This envelope does not take into account the localization phenomena. However, it can appears just in the case of finite model simulation with 10 RV. For high gamma values, the chances of appearing this situation is higher.

It is also possible to observe in figures 7 (b) and 7(d) that there is a branch correspondent to a longitudinal wave that inhibits the appearance of two others bandgaps which can be verified by the appearance of on figures 7 (a) and 7 (c).

5 Conclusion

A low computational cost three-dimensional periodic structure truss was used as a numerical example. Firstly, solutions for finite and infinite structures were found likewise their frequency response and dispersion diagrams, respectively. This structure was discretized by a bar finite element with 3 degrees of

freedom per node. A number of cells equals to ten has been selected for the finite structure. This choice was made in order to obtain credible location of the attenuation frequency zones without substantially increasing the computational cost.

The localization phenomenon was identified related to a place with strong impedance mismatch. This important remark was clarified and it explains the behavior of uncertainties in this kind of repetitive structure. A relevant impedance mismatch, which highly differs from the other cells, localized in some place of the repetitive structure can reveal interesting properties.

An uncertainty analysis was performed using the finite and infinite models of this structure. The added joint mass and inductance values were purposely chosen as random variables with a Gaussian probability density function owning a mean and standard deviation as stochastic properties.

The choice of this probability distribution is explained due to its facility of understanding. Although the mass and inductance values may achieve negative values for this model, a strongly high value of standard deviation is necessary.

A coefficient of variation, namely gamma, was specified to vary the standard deviation as a percentage of the mean value. Numerous Monte Carlo Simulations with Latin Hypercube were conducted until their convergences for each value of the coefficient mentioned before.

The results for infinite and finite models are different. The results for infinite structures are not completely reliable since the same uncertainty is repeated indefinitely. The results for finite structures are more reliable since the uncertainty is considered ten times for the finite structure with ten cells.

The confidence envelope for the complete structure with ten stochastic variables is narrower than those found with one random variable. Besides, they are more reliable due to the model being closer to reality for the same case. The fact of considering ten random variables, instead of one, proves that the uncertainties self-compensate and the periodic structures are intrinsically tough.

Finally, a more accurate and reliable robust smart bandgap was obtained.

Acknowledgements

The authors are grateful to the Brazilian National Research Council - CNPq and to the National Institute of Science and Technology of Smart Structures in Engineering - INCT-EIE for the financial support to their research work. This work was realized in the context of ANR-12-JS09-008-Covia project, in cooperation with the Labex ACTION (ANR-11-LabX-0001-01).

References

[1] F. Graff, *Wave Motion in Elastic Solids*. Dover Publications Inc. New York. (1975).

[2] G. Floquet, *Sur les équations différentielles linéaires à coefficients périodiques*. Annales scientifiques de l'ENS, Vol.129(1), (1883), pp. 47-88.

[3] D.J. Mead, *Wave Propagation in continuous periodic structures: Research contributions from Southampton, 1964-1995*. Journal of Sound and Vibration, Vol. 190(3), (1996), pp. 243-268.

[4] M. I. Hussein, M. J. Leamy, M. Ruzzene, *Dynamics of Phononic Materials and Structures: Historical Origins, Recent Progress, and Future Outlook*, ASME, (2014), Vol. 66.

[5] O. Thorp, M. Ruzzene, A. Baz, *Attenuation and localization of wave propagation in rods with periodic shunted piezoelectric patches*. Smart Materials and Structures, Vol. 10, (2001), pp. 979-989.

[6] A. Spadoni, M. Ruzzene, K. Cunefare, *Vibration and Wave Propagation Control of Plates with Periodic Arrays of Shunted Piezoelectric Patches*, Journal of Intelligent Material Systems and Structures, Vol. 20 , (2009), pp. 979-990.

[7] Den Hartog, J.P., *Mechanical Vibrations*, McGraw-Hill Book Company, Inc. (1956), 366p.

[8] B.G. Korenev, L.M. Reznikov, *Dynamic Vibration Absorbers*, Theory and Technical Application John Wiley & Sons DVA, (1993).

[9] D.A. Rade, V. Steffen Jr, *Optimisation of dynamic vibration absorbers over a frequency band*. Mechanical Systems and Signal Processing. Vol. 14 (5), (2000), pp.679-690.

[10] C.C. Claeys, K. Vergote, P. Sas, W. Desmet, *On the potential of tuned resonators to obtain low-frequency vibrational stop bands in periodic panels*, Journal of Sound and Vibration, Vol. 332, (2013), pp. 1418-1436.

[11] J. Signorelli, A.H. Von Flotow, *Wave Propagation, Power flow, and Resonance in a Truss Beam*, Journal of Sound and Vibration, Vol. 126(1), (1988), pp. 127-144.

[12] J. Signorelli, A.H, Von Flotow, *Wave Propagation in Periodic Truss Structures*, AIAA, (1987), pp. 900-909.

[13] C. H. Park, A. Baz, *Vibration Control of Beams with Negative Capacitive Shunting of Interdigital Electrode Piezoceramics*, Journal of Vibration and Control, Vol. 11, (2005), pp. 331-346.

[14] E. Baravelli, M. Ruzzene, *Internally resonating lattices for bandgap generation and low-frequency vibration control*, Journal of Sound and Vibration, Vol. 332, (2013), pp. 6562-6579.

[15] S. Taniker, C. Yilmaz, *Phononic gaps induced by inertial amplification in BCC and FCC lattices*, Physics Letters A, Vol. 377, (2013), pp. 1930-1936.

[16] Z.-J Wu, F.-M Li, C. Zhang, *Vibration properties of piezoelectric square lattice structures*, Mechanics Research Communications, Vol. 62. (2014), pp. 123-131.

[17] Y. Yong, Y.K. Lin, *Propagation of decaying waves in periodic and piecewise periodic structures of finite length*, Journal of Sound and Vibration, Vol. 129, No. 2, (1989), pp. 99-118.

[18] Y. Yong, Y.K. Lin, *Dynamics of Complex Truss-Type Structures*, AIAA, Vol. 28, No. 7, (1990), pp.-1258.

[19] S.S. Mester, H. Benaroya, *Periodic and Near-Periodic Structures*. Shock and Vibration, Vol. 2(1), pp. 69-65 (1995).

[20] S. Chakraborty, B.K. Roy, *Reliability based optimum design of Tuned Mass Damper in seismic vibration control of structures with bounded uncertain parameters*, Probabilistic Engineering Mechanics, Vol. 26, (2011), pp. 215-221.

[21] D.J. Leo, *Engineering Analysis of Smart Material Systems*, New Jersey: John Wiley & Sons, (2007).

[22] N.W. Hagood, A. Von Flotow, *Damping of Structural Vibrations with Piezoelectric Materials and Passive Electrical Networks*, Journal of Sound and Vibration, Vol. 146(2), (1991), pp. 243-268.

[23] T.P. Sales; D.A. Rade; L.C.G de Souza, *Passive vibration control of flexible spacecraft using shunted piezoelectric transducers*. Aerospace Science and Technology, Vol. 29 (1), (2013), pp.493-412.

[24] F. dell'Isola, C. Maurini, M. Porfiri, *Passive damping of beam vibrations through distributed electric networks and piezoelectric transducers: prototype design and experimental validation*. Smart materials and Structures, Vol. 13, (2004), pp. 299-308.

[25] B de Marneffe, A. Preumont, *Vibration damping with negative capacitance shunts: theory and experiment*. Smart materials and Structures, Vol. 17, (2008), 9p.

[26] F. Casadei, B.S. Beck, K.A. Cunefare, M. Ruzzene, *Vibration control of plates through hybrid configurations of periodic piezoelectric shunts*. Journal of Intelligent Material Systems and Structures, Vol. 23(10), pp. 1169-1177 (2012)

[27] B. Lossouarn, J.F. Deü, M. Aucejo, *Multimodal vibration damping of a beam with Periodic array of piezoelectric patches connected to a passive electrical network*. Smart Materials and Structures, Vol. 24 (11), (2015), 14p.

[28] F. Tateo, M. Collet, M. Ouisse, M.N. Ichchou, K.A. Cunefare, P. Abbe, *Experimental characterization of a bi-dimensional array of negative capacitance piezo-patches for vibroacoustic control*. Journal of Intelligent material Systems and Structures, Vol. 26, (2014), pp. 952-964.

[29] F. Tateo, M. Collet, M. Ouisse, K.A. Cunefare, *Design variables for optimizing adaptive metacomposites made of shunted piezoelectric patches distribution*. Journal of Vibration and Control, Vol. 22, (2014), pp. 1838-1854.

[30] A. Preumont, *Vibration Control of Active Structures*, Second edition, Kluwer Academic Publishers, (2004).

[31] R. Orris, M. Petyt, *A finite element study of harmonic wave propagation in periodic structures*. Journal of Sound and Vibration, Vol. 33(2), (1974), pp. 223-236.

[32] R.M. Mace, E. Manconi, *Modelling wave propagation in two-dimensional structures using finite element analysis*. Journal of Sound and Vibration. Vol. 318, (2008), pp. 884-902.

[33] R.E., Melchers, *Structural Reliability Analysis and Prediction*, Second edition, New York: John Wiley & Sons, (1999).

[34] M., Lemaire, *Structural Reliability*, ISTE, (2009).

[35] A. Haldar, S. Mahadevan, *Probability, Reliability and Statistical Methods in Engineering Design*, New York: John Wiley & Sons, (2000).

[36] S.K. Choi, R.V. Grandhi, R.A. Canfield, *Reliability-Based Structural Design*, London: Springer-Verlag (2007), 306p.